Title: Artificial impact crater formed on the asteroid 162173 Ryugu in the gravity-dominated regime

Authors: M. Arakawa[1*], T. Saiki[2], K. Wada[3], K. Ogawa[1], T. Kadono[4], K. Shirai[2], H. Sawada[2], K. Ishibashi[3], R. Honda[5], N. Sakatani[2], Y. Iijima[2§], C. Okamoto[1§], H. Yano[2], Y. Takagi[6], M. Hayakawa[2], P. Michel[7], M. Jutzi[8], Y. Shimaki[2], S. Kimura[9], Y. Mimasu[2], T. Toda[2], H. Imamura[2], S. Nakazawa[2], H. Hayakawa[2], S. Sugita[10], T. Morota[10], S. Kameda[11], E. Tatsumi[12], Y. Cho[10], K. Yoshioka[10], Y. Yokota[2], M. Matsuoka[2], M. Yamada[3], T. Kouyama[13], H. Suzuki[14], C. Honda[15], Y. Tsuda[2], S. Watanabe[16,2], M. Yoshikawa[2], S. Tanaka[2], F. Terui[2], S. Kikuchi[2], T. Yamaguchi[2†], N. Ogawa[2], G. Ono[17], K. Yoshikawa[17], T. Takahashi[2], Y. Takei[2], A. Fujii[2], H. Takeuchi[2], Y. Yamamoto[2], T. Okada[2], C. Hirose[17], S. Hosoda[2], O. Mori[2], T. Shimada[2], S. Soldini[2], R. Tsukizaki[2], T. Iwata[2], M. Ozaki[2], M. Abe[2], N. Namiki[18], K. Kitazato[15], S. Tachibana[10], H. Ikeda[17], M. Ishiguro[19], N. Hirata[15], N. Hirata[1], R. Noguchi[2].

Affiliations:

1. Kobe University, Kobe 657-8501, Japan.
2. Institute of Space and Astronautical Science, Japan Aerospace Exploration Agency, Sagamihara 252-5210, Japan.
3. Planetary Exploration Research Center, Chiba Institute of Technology, Narashino 275-0016, Japan.
4. University of Occupational and Environmental Health, Kitakyusyu 807-8555, Japan.
5. Kochi University, Kochi 780-8520, Japan.
6. Aichi Toho University, Nagoya 465-8515, Japan.
7. The Côte d'Azur Observatory, 06304 Nice Cedex 4, France.
8. University of Bern, 3012 Bern, Switzerland.
9. Tokyo University of Science, Noda 278-8510, Japan.
10. The University of Tokyo, Tokyo 113-0033, Japan.
11. Rikkyo University , Tokyo 171-8501, Japan.
12. University of La Laguna, 38205 San Cristóbal de La Laguna, Spain.
13. National Institute of Advanced Industrial Science and Technology, Tokyo 135-0064, Japan.
14. Meiji University, Kawasaki 214-8571, Japan.
15. The University of Aizu, Aizu-Wakamatsu 965-8580, Japan.
16. Nagoya University, Nagoya 464-8601, Japan.
17. Research and Development Directorate, Japan Aerospace Exploration Agency, Sagamihara 252-5210, Japan.
18. National Astronomical Observatory of Japan, Mitaka 181-8588, Japan.
19. Seoul National University, Seoul 08826, Korea.

Seoul National University, Seoul 08826, Korea.
[*]Corresponding author: E-mail: masahiko.arakawa@penguin.kobe-u.ac.jp
[†]Current affiliation: Mitsubishi Electric Corporation, Kamakura 247-8520, Japan.
[§]Deceased.

Abstract: The Small Carry-on Impactor onboard Hayabusa2 performed the first impact experiment on a small asteroid, which allowed to study the crater formation mechanism on the rubble pile asteroid Ryugu. Here, we show that an artificial impact crater with a diameter >10 meters was formed, which has a semi-circular shape, a deposition rim and a central pit. The Deployable CAMera 3 recorded for >18 minutes images of the impact outcome, showing the ejecta curtain growth and the ejecta deposition on the surface. The observed ejecta curtain was asymmetric and heterogeneous, and a detachment of the whole curtain from the surface was never observed. These observations indicate that the artificial crater was formed in the gravity-dominated regime with possible implications on Ryugu's surface age. [122 words]

One Sentence Summary: An artificial impact crater with a diameter >10 meters was formed with asymmetric and heterogeneous ejecta curtains on the asteroid Ryugu. [118 characters]

Main Text: The near-earth asteroid 162173 Ryugu was explored by the Japanese spacecraft Hayabusa2 since June 2018, providing the first detailed images of a small asteroid belonging to the C taxonomic class and the entire surface was found to be covered with countless boulders with a maximum size >100 m (*1*, *2*). The regolith layer on the surface of Ryugu under microgravity conditions of about 1×10^{-4} m s^{-2} was expected to have strength originating from cohesion forces between regolith grains, and the maximum strength of the surface layer was estimated theoretically to be 1 kPa (*3*). In principle, this surface strength should control the crater formation process under microgravity conditions and consequently reduce drastically the impact crater size compared to the expected size on a strengthless surface (*4*). Crater scaling laws used to predict the crater size formed by hypervelocity impacts on small bodies as a function of impact conditions are necessary in order to construct a crater chronology on asteroid Ryugu and depending on the considered law, the surface age could differ by more than one order of magnitude (*1*).

A Small Carry-on Impactor (SCI) was equipped with Hayabusa2 spacecraft in order to form an artificial impact crater (SCI crater, hereafter) on the surface of Ryugu. The SCI crater enables us to access the asteroid interior for investigating the subsurface properties by remote sensing and for acquiring subsurface material by active sampling (*5*, *6*). Furthermore, the SCI impact is the first precious opportunity to study the impact crater formation process under a microgravity environment on a real asteroid surface. In particular, conventional crater scaling laws for the crater size and the ejecta velocity distribution can be verified at the actual size of an asteroid, and the SCI impact is a unique and valuable anchor to compare with numerous numerical simulations of the impact cratering processes in a microgravity environment (*7*). Its results, in particular the relation between projectile size and crater size, can thus be applied to natural craters on Ryugu in order to evaluate with higher reliability the crater chronology.

The SCI operation was carried out on 5 April, 2019 and was successfully accomplished to form a visible artificial impact crater on Ryugu. The production and evolution of impact ejecta from the surface of Ryugu were also successfully observed by a Deployable CAMera 3 (DCAM3) (*8*). About 2 weeks after the SCI impact, Hayabusa2 and its Optical Navigation Camera-Telescopic (ONC-T) looked for the SCI crater at an altitude of 1.7 km, then found it at a latitude 7.9° N and a longitude 301.3° E as shown in Fig. 1A and B, very close to the aiming point at a latitude 6.00° N and a longitude 303.00° E in a north area of the equatorial ridge. The impact angle was estimated to be ~60° measured from the local horizontal surface (*8*).

Both the aiming point area of the SCI impact and the SCI crater were observed by ONC-T before and after the SCI impact at an altitude of 1.7 km (Fig. 1A and B). The comparison of both images with a resolution of ~17 cm/pixel reveals a large impact crater (Fig. 1B). It is noticeable

that a dozen of boulders larger than several 10 cm in the middle area in Fig. 1A were driven away from the surface, and more impressively, a huge boulder with a size of 5 m (named as M.B.) initially buried underground before the impact was excavated and moved about 3 m toward the northwest and upward more than 1 m above the initial surface after the impact. In the image before the impact, the boulder M.B. lied adjacent to the other huge boulder located at the right side in the image (named as S.B.) (Fig. 1A), but this boulder S.B. was hardly moved by the SCI impact. This may be due to the fact that S.B. was part of a bedrock buried below the crater floor at some depth, preventing any motion as a result of the SCI impact. We thus speculate that S.B. and its thick bedrock stopped the crater growth toward the southeast. The crater morphology profile can be seen in a Digital Elevation Map (DEM) (Fig. 2) (*8*). We can recognize a deposition rim surrounding the SCI crater and the height of the rim is measured to be as high as 40 cm in Fig. 2. The deposition rim is a strong evidence for the crater formation occurring in the gravity-dominated regime (*9*).

In order to measure the shape of the SCI crater, we used the DEM to produce an ortho-corrected image, on which we could then trace the top of the deposition rim and determine the crater shape (Fig. 1C). We found that the SCI crater has a semicircular shape with a major axis of 17±1 m corresponding to the crater rim diameter (D_{rim}). This shape is not an effect of the oblique impact but is rather due to the blocking effect of bedrock, such as S.B. lying southeast of the impacted region (Fig. 1B) (*8*). Considering the usual symmetry of the crater formation process, we assume that the SCI impact point is the center of the semicircle showing the SCI crater rim. Since the crater diameter (D) is conventionally measured at an initial surface elevation and is different from the crater rim diameter, we used the empirical equation $D=D_{\mathrm{rim}}/1.3$ to estimate the crater diameter as done in (*10*). Thus, we determine the crater radius of the SCI crater to be 6.5±0.4 m, and this crater radius was confirmed by the DEM (Fig. 2A).

We found a pit close to the impact point on the crater floor (*8*). The pit entrance is at a depth of 1.7 m from the initial surface (Fig. 2B); the diameter and the depth of the pit is >2 m and 0.6 m, respectively. The pit has a conical shape similar to a simple crater in laboratory experiments (*9*). A central pit is commonly observed in tiny craters on lunar surface because the lunar subsurface has a layered structure consisting of a relatively hard layer covered with cohesionless regolith (*11*). Therefore, the pit might result from the SCI impact on a subsurface layer with a cohesion strength. The cohesion strength of this subsurface layer is estimated to be between 130 Pa and 300 Pa (*8*). Since the depth of the pit is measured to be 2.7 m from the rim top, the depth to rim diameter ratio of the SCI crater is 0.16. This value is almost similar to that of the natural craters found on Ryugu from 0.14 to 0.2 (*1*).

Inside the crater, although several large and middle size boulders (1.9 m to 0.6 m) are placed on it, the wall shows an absence of roughness and therefore looks smooth (Fig. 1D). These boulders are buried inside the wall and could have been exposed by the excavation flow during the crater growth. The crater wall has a different size frequency distribution of boulders from that on the nearby area (Fig. S3): the number density of boulders on the wall is 1/3 of that in the C01-C region (10°N, 300°E), about 20 m west of the impact point, although the surface condition in this region could be similar to the impact point before the SCI impact in submeter resolution. Thus, the SCI crater wall might be filled with fine regolith. Assuming that the crater wall represents the subsurface structure revealed by the excavation flow, we conclude that the subsurface layer is dominated by fine regolith.

DCAM3 successfully observed impact ejecta generated by the SCI impact from the beginning to more than 18 minutes after the impact. Fig. 3A-F shows the successive images

taken by DCAM3 from 5 s to 498 s after the impact. We see a very clear narrow white line, showing the impact ejecta curtain growing from the surface toward the north with an angle of 40° measured from the surface at 5 s (Fig. 3A). The impact ejecta curtain was observed to be asymmetric in the early stage of the crater formation: an ejecta growth toward the south seems absent, but a faint scattered light showing low speed ejecta is visible at the root of the ejecta curtain.

At 36 s and 100 s, the northward ejecta curtain becomes clearer and extends further. Besides the northward ejecta curtain, two more discrete ejecta curtains are recognized in these images: they are visible at the middle and left of the ejected region (Fig. 3B, C). At the root of the ejecta curtain, a continuous ejecta curtain shown as a shadow begins to grow both vertically and horizontally, and this ejecta growth could originate from the crater growth together with the continuous excavation of the subsurface material.

The three discrete ejecta curtains previously observed grow more and more in both size and thickness, and become more visible at 192 s (Fig. 3D). It seems that the crater growth still continues at this time. One more discrete ejecta curtain can be recognized as a dark shadow in this image at the center of the ejected region and looks growing toward the line of sight of DCAM3, but a visible ejecta curtain cannot be observed in the southeast area. The surface of Ryugu is covered with many large boulders with a power law size distribution and they are also buried in the subsurface (*1*). The SCI impact area was also covered with boulders >0.6 m and some of them had most of their volume buried in the ground (Fig. 1A). These boulders could cause a heterogeneous ejecta growth, which would then result in discrete ejecta curtains, i.e., the boulders on or under the surface might stop the excavation flow, separating the ejecta curtain into four components.

In general, a detachment of the whole ejecta curtain from the ground occurs during crater formation in the strength regime but not in the gravity regime (*5*). In fact, a detachment of the ejecta curtain was never observed in the successive images until 192 s where it was observed, and furthermore we confirmed in the other recorded images that the ejecta detachment did not occur through the SCI crater formation process during the whole 498 s. We propose, therefore, that the SCI crater was formed not in the strength, but in the gravity-dominated regime.

The distribution of discrete ejecta curtains around the SCI impact crater was analyzed by using the image at 192 s together with ONC-T images of the SCI crater area obtained before the impact. The direction and the covered area of each discrete ejecta curtain on Ryugu's surface were identified on the images taken by ONC-T with the reference of DCAM3 line of sight. Fig. 4B shows the distribution of the ejecta curtains mapped on an ONC-T surface image; each numbered sector on the map corresponds to the numbered discrete ejecta curtain (Fig. 4A), while the continuous ejecta curtain is displayed by a semicircle at the center. It is quite impressive that the whole ejecta curtain, including the discrete curtains as well as the continuous curtain, was only distributed on the northwest-side. This ejecta curtain distribution map can be compared with an ONC-T v-band reflectance difference map (*8*) in this area as shown in Fig. 4C: the darker colored area shows the larger decrease of the reflectance factor and this area is believed to be covered with a relatively thick ejecta deposit. This darkened area is asymmetric against the crater: there are 4 discrete extended areas and there is no or only a very faint black colored area in the southeast area of the crater. These features of the reflectance difference map are very well consistent with our ejecta distribution map, so that we are convinced that the map represents the spatial distribution of the ejecta deposit and the ejected subsurface material corresponds to a low reflectance on Ryugu.

At 396 s and 498 s, a surface pattern of Ryugu behind ejecta curtains can be completely seen (Fig. 3E, F), showing that the optical thickness of the ejecta curtain at those times was rather thinner than that at 192 s. In these images, we see a deep gray elliptic area surrounded by the discrete ejecta curtains. We consider that the deep grey color of this area is an intrinsic color of the surface, and we suggest that it represents the excavated area and/or the ejecta deposit area. Since the crater growth would already stop after 300 s (*8*), the ejecta curtains observed in these images were on the way to just falling onto the surface in each ballistic trajectory. The elliptic area in the image at 498 s was analyzed and the major axis of the ellipse was determined to be 36 m.

Since the structures of the SCI crater and the ejecta curtains as described above support the interpretation that the SCI crater was formed in the gravity-dominated regime, we calculate the SCI crater radius using the conventional π scaling law applied for a typical sand (cohesionless) surface (*8*). The calculated radius is 6.87 m, which is slightly larger than that of the observed SCI crater of 6.5 m. Although the SCI impact crater is about 5 % smaller than that calculated for sand, it can only be formed on a cohesionless surface such as one made of sand, because even a small amount of cohesion would limit the crater growth in this microgravity environment and prohibits the crater diameter to be >10 m (*8*), as observed. Then, we can reasonably conclude that the surface of Ryugu must be composed of sand-like cohesionless material. According to the π scaling law, we can estimate the optimal k_1 value applicable to the surface of Ryugu by adopting the SCI crater radius of R = 6.5 m (*8*); we obtain k_1 = 0.56 if we assume that other parameters related to the coupling parameter are the same as typical values for sand, and they could be suitable for cohesionless targets at high impact velocities: $\mu = 0.41$ and $\nu = 0.4$ (*8*, *10*). In that case, the following crater size scaling law is the most suitable one for the surface of Ryugu; $\pi_R = 0.56 \cdot {\pi_2}^{-0.17} {\pi_4}^{0.0014}$. This result could directly affect the results of the crater chronology on Ryugu studied by Sugita et al. (2019) (*1*). Based on collision frequency models for the main belt (*13*, *14*), two estimates of the surface age of Ryugu have been obtained: one is 1.58×10^8 years for a surface composed of a dry-soil with cohesion and another is 8.9×10^6 years for a cohesionless surface. Our crater size scaling law built from the crater size produced by the SCI, supports the younger age estimated for a cohesionless surface. Moreover, it suggests that the crater retention age of the top 1 m of the surface layer is ~1×10^5 years or younger when crater production functions on Ryugu for near-Earth orbits based on (*12*, *13*) was used (*8*). The age and evolution history of Ryugu's surface should be refined by using our scaling law that matches an actual experiment on Ryugu's surface provided by the SCI. [2500 words]

References and Notes:

1. S. Sugita et al., The geomorphology, color, and thermal properties of Ryugu: Implications for parent-body processes. *Science* **364**, eaaw0422 (2019). doi: 10.1126/science.aaw0422
2. S. Watanabe et al., Hayabusa2 arrives at the carbonaceous asteroid 162173 Ryugu–A spinning top-shaped rubble pile. *Science* **364**, 268–272 (2019). doi: 10.1126/science.aav8032
3. K. Wada et al., Asteroid Ryugu before the Hayabusa2 encounter. *Prog. Earth Planet. Sci.* **5**, 82 (2018). doi: 10.1186/s40645-018-0237-y
4. K. Holsapple, I. Giblin, K. Housen, A. Nakamura, E. Ryan, Asteroid impacts: Laboratory experiments and scaling laws. in Asteroids III, University of Arizona Press, Tucson, pp. 443–462 (2002).
5. M. Arakawa et al., Scientific objectives of Small Carry-on Impactor (SCI) and Deployable

Camera 3 Digital (DCAM3-D): observation of an ejecta curtain and a crater formed on the surface of Ryugu by an artificial high-velocity impact. *Space Sci. Rev.* **208**, 187–212 (2017). doi: 10.1007/s11214-016-0290-z
6. S. Tachibana et al., Hayabusa2: Scientific importance of samples returned from C-type near-Earth asteroid (162173) 1999 JU3. *Geochem. J.* **48**, 571–587 (2014). doi: 10.2343/geochemj.2.0350
7. M. Jutzi, K. Holsapple, K. Wünneman, P. Michel, Modeling asteroid collisions and impact processes. in Asteroids IV, University of Arizona Press, Tucson, pp. 679–699 (2015). doi: 10.2458/azu_uapress_9780816532131-ch035
8. Materials and Methods are available as Supplementary Materials.
9. H. J. Melosh, Impact cratering: A geologic process. Oxford University Press, New York (1989).
10. K. R. Housen, K. A. Holsapple, Ejecta from impact craters. *Icarus* **211**, 856–875 (2011). doi: 10.1016/j.icarus.2010.09.017
11. Z. Yue et al., Lunar regolith thickness deduced from concentric craters in the CE-5 landing area. *Icarus* **329**, 46–54 (2019). doi: 10.1016/j.icarus.2019.03.032
12. W. F. Bottke Jr. et al., The fossilized size distribution of the main asteroid belt. *Icarus* **175**, 111–140 (2005). doi: 10.1016/ j.icarus.2004.10.026
13. D. P. O'Brien, R. Greenberg, The collisional and dynamical evolution of the main-belt and NEA size distributions. *Icarus* **178**, 179–212 (2005). doi: 10.1016/j.icarus.2005.04.001
14. T. Saiki et al., The small carry-on impactor (SCI) and the Hayabusa2 impact experiment. *Space Sci. Rev.* **208**, 165–186 (2017). doi: 10.1007/s11214-016-0297-5
15. K. Ogawa et al., System configuration and operation plan of Hayabusa2 DCAM3-D camera system for scientific observation during SCI impact experiment. *Space Sci. Rev.* **208**, 125–142 (2017). doi: 10.1007/s11214-017-0347-7
16. K. Ishibashi et al., Performance of Hayabusa2 DCAM3-D camera for short-range imaging of SCI and ejecta curtain generated from the artificial impact crater formed on asteroid 162137 Ryugu (1999JU3). *Space Sci. Rev.* **208**, 213–238 (2017). doi: 10.1007/s11214-016-0298-4
17. D. E. Gault, J. A. Wedekind, Experimental studies of oblique impact. *Proc. Lunar Planet. Sci. Conf.* **9**, 3843–3875 (1978).
18. R. Szeliski, Computer vision: Algorithms and applications. Springer, London (2010). doi: 10.1007/978-1-84882-935-0
19. W. Schwanghart, D. Scherler, TopoToolbox2-MATLAB-based software for topographic analysis and modeling in Earth surface sciences. *Earth Surf. Dyn.* **2**, 1-7 (2014). doi: 10.5194/esurf-2-1-2014
20. H. M. B. Al-Hashemi, O. S. B. Al-Amoudi, A review on the angle of repose of granular materials. *Powder Technol.* **330**, 397–417 (2018). doi: 10.1016/j.powtec.2018.02.003
21. D. E. Maxwell, Simple Z model of cratering, ejection, and the overturned flap. in Impact and explosion cratering: Planetary and terrestrial implications, Pergamon, New York, pp. 1003–1008 (1977).
22. K. R. Housen, R. M. Schmidt, K. A. Holsapple, Crater ejecta scaling laws: Fundamental forms based on dimensional analysis. *J. Geophys. Res. Solid Earth* **88**, 2485–2499 (1983). doi: 10.1029/JB088iB03p02485

Acknowledgments: Hayabusa2 was developed and built under the leadership of Japan Aerospace Exploration Agency (JAXA), with contributions from the German Aerospace Center

(DLR) and the Centre National d'Études Spatiales (CNES), and in collaboration with NASA, and other universities, institutes, and companies in Japan. SCI and DCAM3 were developed by JAXA, Kobe University, Chiba Institute of Technology, University of Occupational and Environmental Health, Kochi University, and other universities, institutes, and companies in Japan. M.Ar. thanks Dr. Minami Yasui for her help of conducting laboratory impact experiments. K.W. is grateful to Dr. Hiroshi Kimura for discussing the observational possibility of ejecta curtain. **Funding:** This study was supported by KAKENHI from the Japanese Society for Promotion of Science (JSPS) (Grant Nos. JP16H04041, JP17H06459, JP15K05273, JP19H01951, JP19H00719) and the JSPS Core-to-Core program "International Network of Planetary Sciences." P.M. acknowledges funding support from the French space agency CNES and from Academies of Excellence: Complex systems and Space, environment, risk, and resilience, part of the IDEX JEDI of the Université Côte d'Azur. **Author contributions:** M.Ar. coordinated coauthor contributions; led the SCI and DCAM3 data acquisition, analyses, and interpretations; and wrote the paper, with contributions from K.W., K.O., T.Ka., K.S., K.I., R.H., N.S., P.M., M.J., and Y.S. SCI operations: T.Sa., K.W., T.Ka., K.S., Y.I., C.O., H.Y., Y.Taka., M.H., H.Im., and N.H. (Aizu) DCAM3 data acquisitions and reductions: K.W., K.O., K.S., H.Sa., K.I., R.H., N.S., Y.I., S.Kim., Y.M., T.To., S.N., and H.H. ONC data aqcuisitions and reductions: H.Sa., R.H., N.S., M.H., S.Su., T.M., S.Ka., E.T., Y.C., K.Yoshio., Y.Yo., M.M., M.Ya., T.Ko., H.Su., and C.Ho. Image analysis: K.W., K.O., T.Ka., K.S., K.I., R.H., N.S., and Y.S. Spacecraft operations: T.Sa., K.O., K.S., H.Sa., R.H., N.S., H.Y., M.H., Y.M., S.N., Y.Ts., S.W., M.Yo., S.Tan., F.T., S.Kik., T.Y., N.O., G.O., K.Yoshiz., T.Ta., Y.Take., A.F., H.T., Y.Ya., T.O., C.Hi., S.H., O.M., T.Sh., S.So., R.T., T.I., M.O., M.Ab., N.N., K.K., S.Tac., H.Ik., and M.I. Shape modeling: K.S., Y.S., N.H. (Aizu), N.H. (Kobe), and R.N. **Competing interests:** Authors declare no competing interests. **Data and materials availability:** The Hayabusa2 ONC and DCAM3 data will be made available through the JAXA Data Archives and Transmission System website (https://www.darts.isas.jaxa.jp/) and is available upon request until posted to the archive.

Supplementary Materials:

Materials and Methods

Figures S1-S5

References (*1-22*)

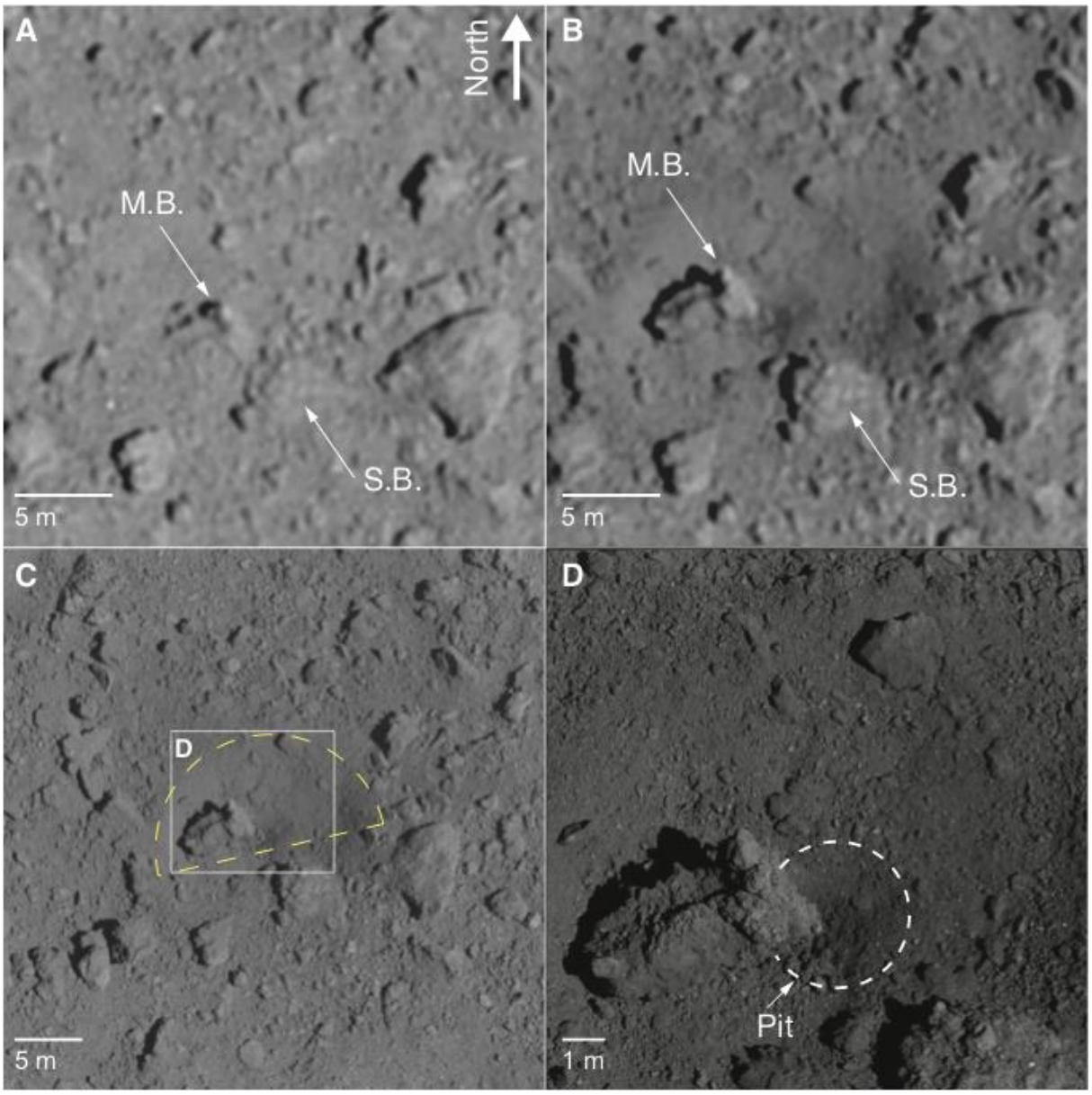

Fig. 1. ONC images of the SCI crater. (A) SCI aiming point area taken at 1.72 km altitude before the impact (hyb2_onc_20190321_192706_tvf_l2b, spatial resolution is four times improved through deconvolution). Large boulders named as Mobile Boulder (M.B.) and Stable Boulder (S.B.) are shown by arrows. (B) SCI aiming point area taken at 1.72 km altitude after the impact (hyb2_onc_20190425_031226_tvf_l2b, deconvolution image). (C) Morphology of the SCI crater (hyb2_onc_20190516_023615_tvf_l2c). This image of the SCI impact area is ortho-corrected. The SCI crater is shown by a yellow dashed semicircle. (D) Close up image of a rectangular area of Fig. 1C taken at 115 m altitude (hyb2_onc_20190613_020217_tvf_l2c). A pit entrance is shown by a dashed curve.

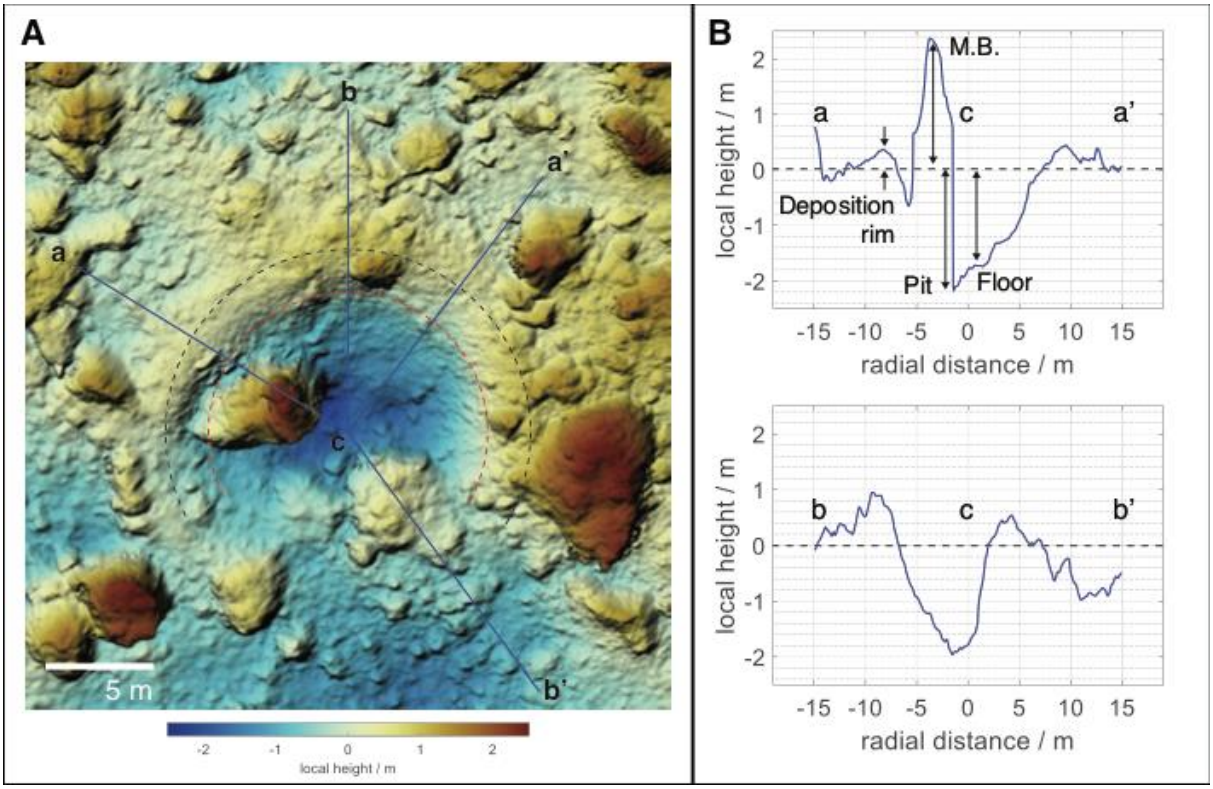

Fig. 2. Topography of the SCI crater. (A) Digital Elevation Map of the SCI impact area. The scale bar is 5m. A black dashed semicircle shows the crater rim with the diameter of 17 m, and a red dashed semicircle shows the crater with the diameter of 13 m. The height of 0 m is a base height which we measured the crater rim from. The contour map in this area is shown in Fig. S2. (B) Cross section of the SCI crater. Traverse lines are shown in Fig. 2A, and the radial distance is measured from a point C. The deposition rim, pit, crater floor, and M.B. are shown in the figure.

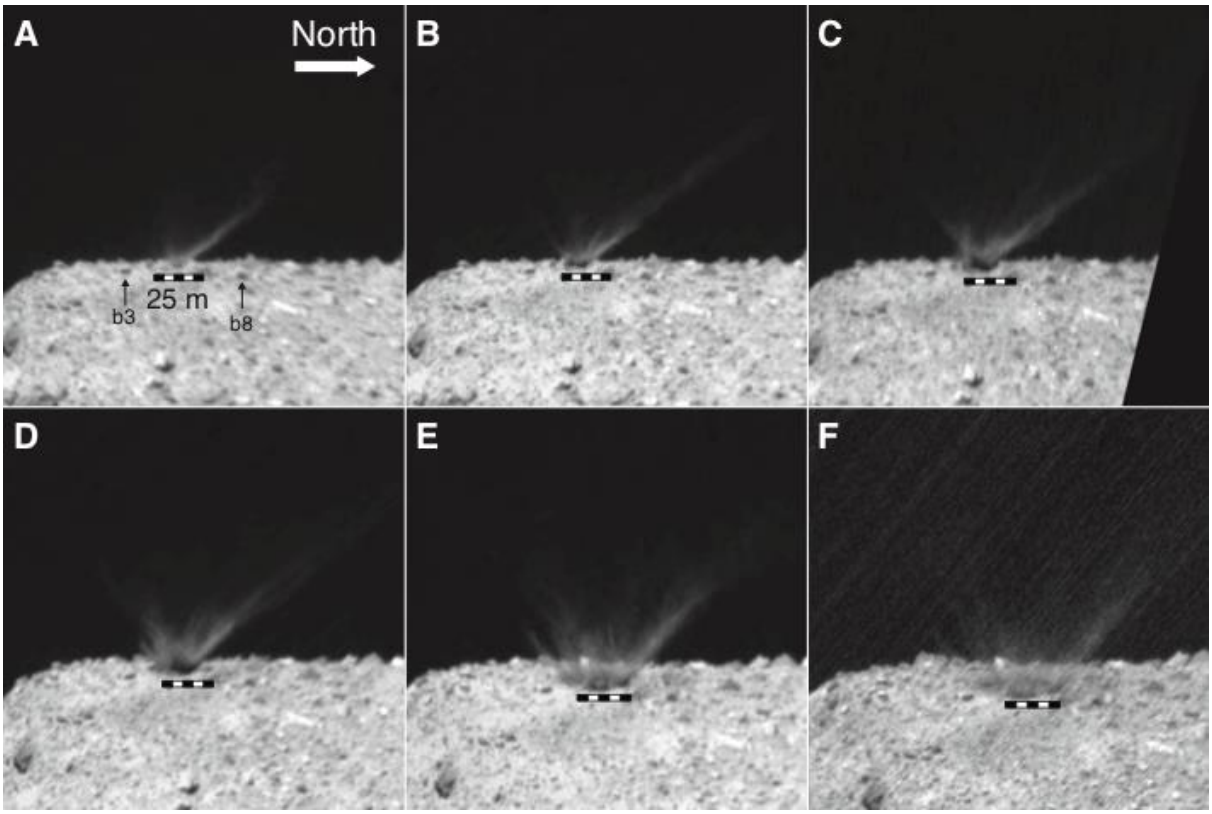

Fig. 3. DCAM3 images of the SCI impact. Elapsed time after the impact are (A) 5 s (hyb2_dcam3d_img-f_01309_l1c), (B) 36 s (hyb2_dcam3d_img-f_01340_l1c), (C) 100 s (hyb2_dcam3d_img-f_01404_l1c), (D) 192 s (hyb2_dcam3d_img-f_01496_l1c), (E) 396 s (hyb2_dcam3d_img-f_01700_l1c), and (F) 498 s (hyb2_dcam3d_img-f_01802_l1c). A scale of 25 m calibrated by the distance between boulders b3 and b8 is show in each image. Note that the impact point moved toward DCAM3 due to the rotation of Ryugu.

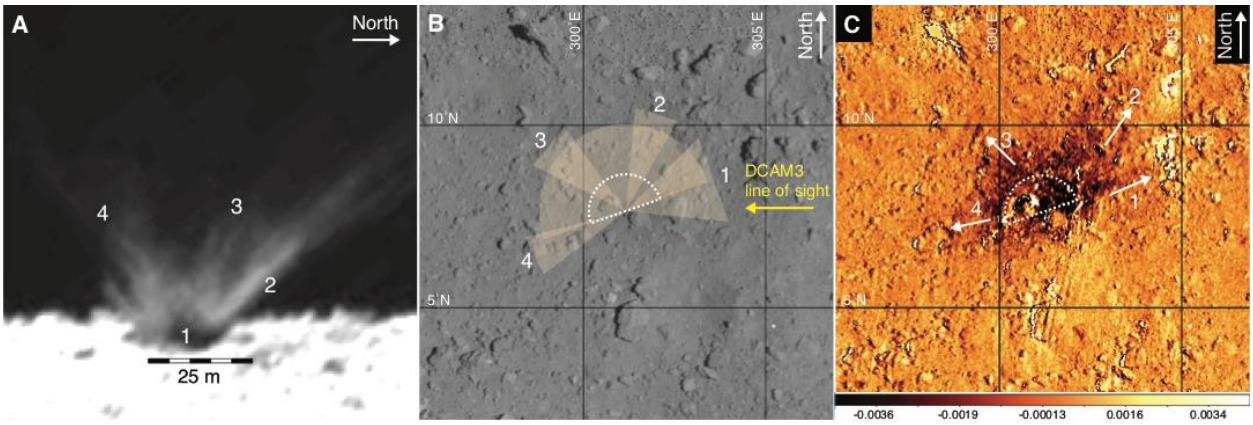

Fig. 4. Distributions of the SCI ejecta curtain. (A) DCAM3 image taken at 192 s. Four discrete ejecta curtains are identified and numbered from 1 to 4 on the image. (B) ONC v-band image map. The line of sight of DCAM3 recording the image of Fig. 4A is shown by an arrow. Numbered discrete ejecta curtains and a continuous ejecta curtain are projected on the ONC image by numbered sectors and a semicircle colored light orange. (C) The map of ONC v-band reflectance factor difference between before and after the SCI impact around the SCI crater. Typical reflectance factor of this area is about 0.018, thus the value of -0.0036 in this map represents the decrease of reflectance by about 20% after SCI impact. There are four discrete extended areas colored darkened numbered from 1 to 4. Please note that the same pre-SCI shape model is used for both of pre- and post-SCI reflectance calculation to detect weak reflectance change due to ejecta deposit outside of the crater.